journal of the mechanical behavior of biomedical materials 104 (2020) 103682

Contents lists available at ScienceDirect

Journal of the Mechanical Behavior of Biomedical Materials

journal homepage: http://www.elsevier.com/locate/jmbbm

Predicting lung mass density of patients with interstitial lung disease and healthy subjects using deep neural network and lung ultrasound surface wave elastography

Boran Zhou [a], Brian J. Bartholmai [a], Sanjay Kalra [b], Xiaoming Zhang [a,*]

[a] Department of Radiology, Mayo Clinic, USA
[b] Department of Pulmonary and Critical Care Medicine, Mayo Clinic, USA

ARTICLE INFO

Keywords:
Deep neural network
Hounsfield unit (HU)
High-resolution computed tomography (HRCT)
Interstitial lung disease (ILD)
Lung density
Lung ultrasound surface wave elastography (LUSWE)
Pulmonary function test (PFT)

ABSTRACT

The Hounsfield unit (HU) obtained from high resolution computed tomography (HRCT) has been used to assess lung pathology. However, lung mass density has not been quantified in vivo noninvasively. The objective of this study was to develop a method for analyzing lung mass density of superficial lung tissue of patients with interstitial lung disease (ILD) and healthy subjects using a deep neural network (DNN) and lung ultrasound surface wave elastography (LUSWE). Surface wave speeds at three vibration frequencies (100, 150 and 200 Hz) from LUSWE and a pulmonary function test (PFT) including predicted forced expiratory volume (FEV1% pre) and ratio of forced expiratory volume to forced vital capacity (FEV1%/FVC%) were used. Predefined lung mass densities based on the HU for ILD patients and healthy subjects (77 in total) were also used to train the DNN model. The DNN was composed of four hidden layers of 1024 neurons for each layer and trained for 80 epochs with a batch size of 20. The learning rate was 0.001. Performances of two types of activation functions in the DNN, rectified linear activation unit (ReLU) and exponential linear unit (ELU), as well as, machine learning models (support vector regression, random forest, Adaboost) were evaluated. The test dataset of wave speeds, FEV1% pre and FEV%/FVC%, was used to predict lung mass density. The results showed that predictions using a DNN with ELU obtained a comparatively better performance in the testing dataset (accuracy = 0.89) than those of DNN with ReLU or machine learning models. This method may be useful to noninvasively analyze lung mass density by using the DNN model together with the measurements from LUSWE and PFT.

1. Introduction

Lung disease is the third-leading killer in the United States, responsible for 1 in 6 deaths (Xu et al., 2010). Nearly 400,000 Americans die annually from lung disease, and death rates from lung disease are increasing even as death rates from other major diseases, including cancer, are declining (Lung Disease Data, 2008). Many lung diseases such as interstitial lung disease (ILD), chronic obstructive pulmonary disease, and acute respiratory distress syndrome are associated with dramatic changes in mechanical properties of the lung. ILD comprises a number of serious diseases in which lung tissue is stiffened and damaged by fibrosis. The Pulmonary Fibrosis Foundation estimates that 200,000 Americans have idiopathic pulmonary fibrosis (Royston et al., 2011). Lung fibrosis can lead to other problems including pulmonary hypertension, respiratory failure, and lung cancer. The incidence and mortality rates of ILD have increased in recent years, and this trend is expected to continue (Lung Disease Data, 2008), especially for ILD-associated systemic diseases (Coultas et al., 1994; Kornum et al., 2008).

High-resolution computed tomography (HRCT) is the clinical standard for diagnosing lung fibrosis (Mathieson et al., 1989; Verschakelen, 2010), but it substantially increases radiation exposure for patients, even when using various techniques to reduce the dose (Mayo, 2009). In addition, the potential for frequent HRCT use is limited by its expense. The forced volume capacity (FVC) level in the pulmonary function test (PFT) has traditionally been regarded as the measure of disease severity, and a decrease in FVC has been associated with increased mortality in ILD. Numerous studies have shown that the extent of emphysema measured by pathology scores in resected lung tissue is well correlated with lung density values obtained from preoperative computed

* Corresponding author. 200 1st St SW, Rochester, MN, 55905, USA.
E-mail address: Xiaoming.Zhang@mayo.edu (X. Zhang).

https://doi.org/10.1016/j.jmbbm.2020.103682
Received 18 October 2019; Received in revised form 2 February 2020; Accepted 6 February 2020
Available online 7 February 2020

Table 1
HU and corresponding mass densities of different soft tissues.

	Hounsfield unit (HU)	Mass density [kg/m^3]
Kidney	20 to 45	1066 ± 56
Liver	60 ± 6	1079 ± 53
Lung	−700 to −600	394 ± 174
Lymph node	10 to 20	1035 ± 7
Midbrain	−120 to −90	911 ± 6
Muscle	35 to 55	1090 ± 52

tomography (CT) of the lung (Gould et al., 1988; Bankier et al., 1999).

Lung ultrasound has been increasingly used in the last decade for diagnosis and prognosis of lung disease (Volpicelli, 2013; Hakimisefat et al., 2010; Zhou and Zhang, 2018a). Its advantages over other imaging modalities are rapidity, no exposure to ionizing radiation, and portability (Zhou and Zhang, 2018b). It is well-known that lung tissue is normally filled with air, and the difference in acoustic impedance between air and tissue is large, resulting in most of the energy of the ultrasound wave reflected from the lung surface. We have developed a lung ultrasound surface wave elastography (LUSWE) technique for noninvasively measuring surface wave speeds of superficial lung tissue (Zhang et al., 2017a, 2018a). Significant differences in surface wave speed of different lung zones between healthy subjects and ILD patients were observed in our previous studies (Zhang et al., 2017b, 2017c, 2018b).

Deep learning has increasingly gained attention as an artificial intelligence strategy in the field of radiology. The deep neural network (DNN) method has widely been used for prediction of housing price and power load (Sousa et al., 2014). The DNN has the capability of extracting high-level features from raw data after using statistical learning over a large amount of data to obtain an effective representation of an input space. The DNN is composed of several layers. The high performance of the DNN model in power load prediction has been reported (Sousa et al., 2014). These observations suggest the potential of using the DNN technique to predict lung mass density.

This study is a continuation of our previous investigation on the prediction of mass density based on LUSWE (Zhou and Zhang, 2018c). Here, we focus on the prediction of lung mass density of the ILD patients and healthy controls based on measurements obtained from LUSWE and PFTs.

2. Materials and methods

2.1. Datasets

This was a retrospective study. From February 2016 to May 2017, there was a cumulative total of 91 patients (M/F: 51/40, mean age: 62.4 ± 12.9 years) and 30 healthy controls (M/F: 16/14, mean age: 45.4 ± 14.6 years) who underwent LUSWE; however, among them, HRCT and PFT data were available for 57 patients (M/F: 30/29, mean age: 60.9 ± 14.3 years) and 20 healthy subjects (M/F: 10/10, mean age: 44 ± 15.4 years).

2.2. Reference standard data: HU and mass density

Literature has shown that the mass density of soft tissue can be determined based on the measured HU values from CT with an accuracy more than 0.04 g/cm^3 (Tanaka et al., 2011). The HUs of ILD patients and healthy controls were quantified with HRCT. In order to calculate lung mass density of ILD patients and healthy subjects, the HU and mass density of different types of soft tissue such as muscle, lung, kidney, liver, midbrain, and lymph node were found in literature (Lepor, 2000; Kuntz and Kuntz, 2006; Kazerooni and Gross, 2004; Twal et al., 2014; Shazly et al., 2015) (see Table 1). Correlation between these two quantities was plotted in Fig. 1. The slope ratio and bias from the linear

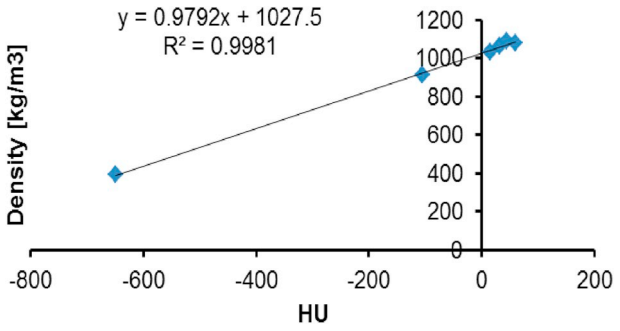

Fig. 1. Linear correlation between HU and mass density of different types of soft tissue.

regression were used to calculate lung mass density of ILD patients and healthy subjects based on their HU values.

2.3. Machine learning algorithm and feature selection

Several machine learning (ML) algorithms, support vector regression, random forest and Adaboost algorithms, were used for predicting lung mass density in this study (Drucker et al., 1997; Liaw and Wiener, 2002; Solomatine and ShresthaAdaBoost., 2004). For support vector regression, the regularization parameters and epsilon were set as 1 and 0.2. For the random forest regressor, the maximum depth was set to 100. For the Adaboost regressor, the number of estimators was set to 100. These ML algorithms were implemented using a scikit-learn library.

Surface wave speeds at three frequencies, predicted forced expiratory volume (FEV1%pre), ratio of forced expiratory volume to forced vital capacity (FEV1%/FVC%), age, and weight of patients and healthy subjects were used as features for training ML models. Random forest revealed feature importance in terms of contribution in percent and showed that the importance of age (<5%) and weight (<5%) were not as high as other features (>10%), so these two features were not used in the training of the DNN model.

2.4. Deep neural network model

The proposed architecture of the DNN model was composed of six fully-connected layers. The DNN model trained by back propagation consisted of five neurons in the input layer, 1024 neurons in each of four hidden layers, and one neuron in the output layer (Fig. 2). Surface wave speeds at three frequencies, FEV1% pre, and FEV1%/FVC% obtained from PFTs(c_{s_100}, c_{s_150}, c_{s_200}, FEV1% pre and FEV1%/FVC%) of lung tissue were imported as input. For our DNN, we used the 'DNNRegressor'. In this study, we evaluated the performances of two activation functions, the rectified linear activation unit (ReLU) and exponential linear unit (ELU).

ReLU is defined as:

$$\mathrm{R}(\mathrm{x}) = \max(0, x) \tag{1}$$

where x is the input to the neuron.

ELU is defined as:

$$\mathrm{f}(\mathrm{x}) = \alpha(e^x - 1), x < 0, \text{ otherwise } \mathrm{f}(\mathrm{x}) = x \tag{2}$$

where α is a parameter and x is the input to a neuron.

To reduce overfitting, regularizer L2 was used for each fully-connected layer. Also, a dropout layer was used in between fully-connected layers to reduce overfitting. The ratio of dropout was 0.5. The training of the DNN is composed of two parts: a training objective and an optimization algorithm to minimize this objective function. In this study, we used an Adam optimizer to minimize the mean square error (MSE) (Kingma and Ba, 2014; Zeiler et al., 2013). Learning rate

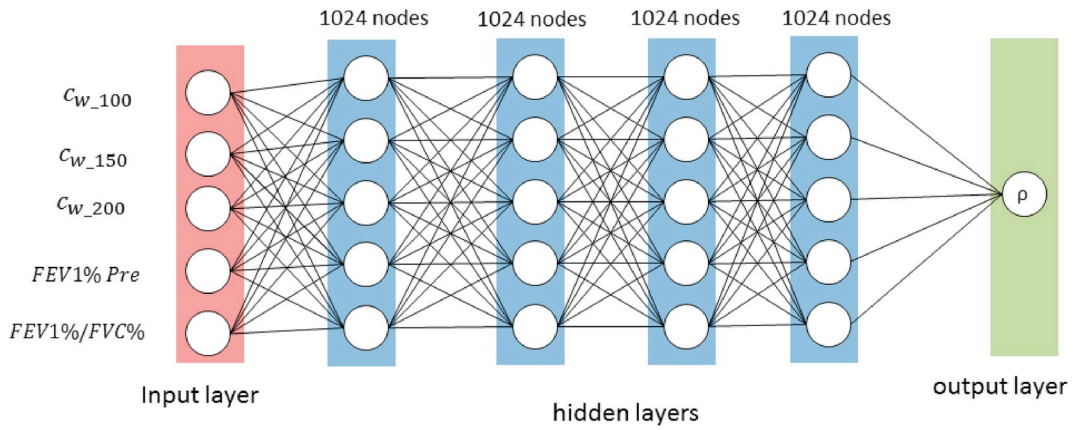

Fig. 2. Schematic of the architecture of the DNN model. Five features are used as inputs, the hidden (fully-connected) layer consists of 1024 neurons, the output layer predicts the lung mass density.

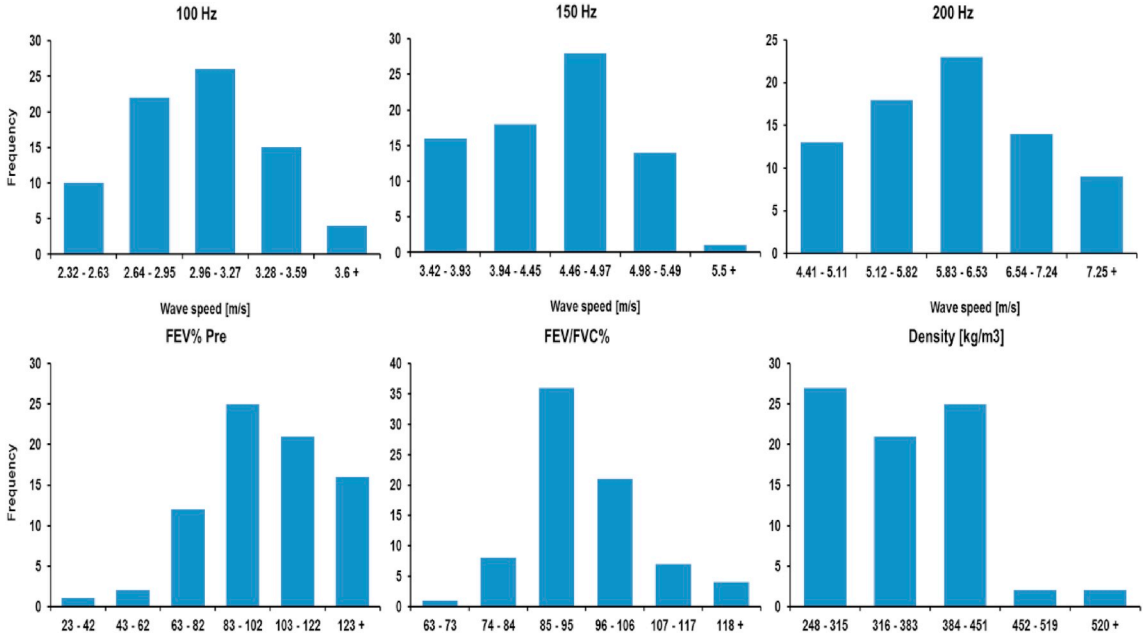

Fig. 3. Distributions of wave speeds at 100, 150 and 200 Hz, FEV% Pre, FEV%/FVC%, and density of dataset.

was 0.001. The neuron in the output layer corresponds to the predicted lung mass density and was compared with the predefined lung mass density (TargetsData). The evaluation of performance of the model was based on a train-validation-test (80/10/10) scheme. The actual training of the approach was carried out on the training dataset, while the validation dataset was used for fine tuning of hyper-parameters; the overall performance of the model was evaluated on the test dataset (Kohavi, 1995).

The trainable weights were initialized with the Xavier initialization (Glorot and Bengio, 2010). The weight updates were performed in mini-batches and the number of samples per batch was set to 20. Training ends when the network does not significantly improve its performance on the validation set for a predefined number of epochs. This number was set to 80 and performance was evaluated in terms of loss and accuracy (Shin et al., 2016; Prim et al., 2016). Loss was the MSE, which is the dissimilarity of the approximated output distribution from the true distribution of labels. $\text{Loss} = \text{MSE} = \frac{1}{n}\sum_{i=1}^{n}(Y_i - \widehat{Y}_i)^2$. Accuracy was calculated in terms of coefficient of determination R2, which is calculated as $R^2 = 1 - \frac{\sum_{i=1}^{n}(Y_i - \widehat{Y}_i)^2}{\sum_{i=1}^{n}(Y_i - \overline{Y})^2}$. Y_i is the training data, $\widehat{Y}_i$ is the prediction from the model, $\overline{Y}$ is the mean value of the training dataset. An improvement was considered significant if the relative increase in performance was at least 0.5%.

The DNN was implemented using the Python API of TensorFlow and TFLearn framework.

2.5. Statistical analysis

The performances of the DNN and ML in predicting lung mass density were evaluated using Pearson's correlation coefficient in comparison to ground-truth lung mass density values obtained based on HU values. The comparisons of correlation coefficients in the testing dataset among different models were performed using Student's independent sample *t*-test. A p value < 0.05 was considered statistically significant.

3. Results

The lung mass density of ILD patients and healthy subjects calculated based on the HU in our study ranged from 180 kg/m^3 to 516 kg/m^3. The magnitude of the lung mass density of the ILD patients (317.68 ± 59.69

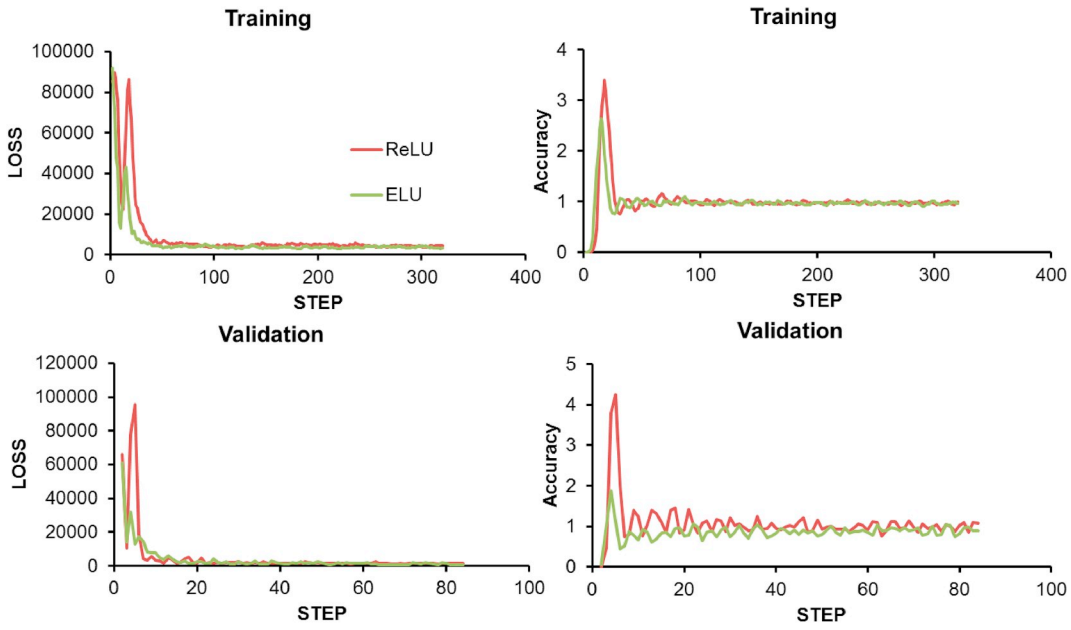

Fig. 4. Loss and accuracy curves of both training and validation processes for different activation functions.

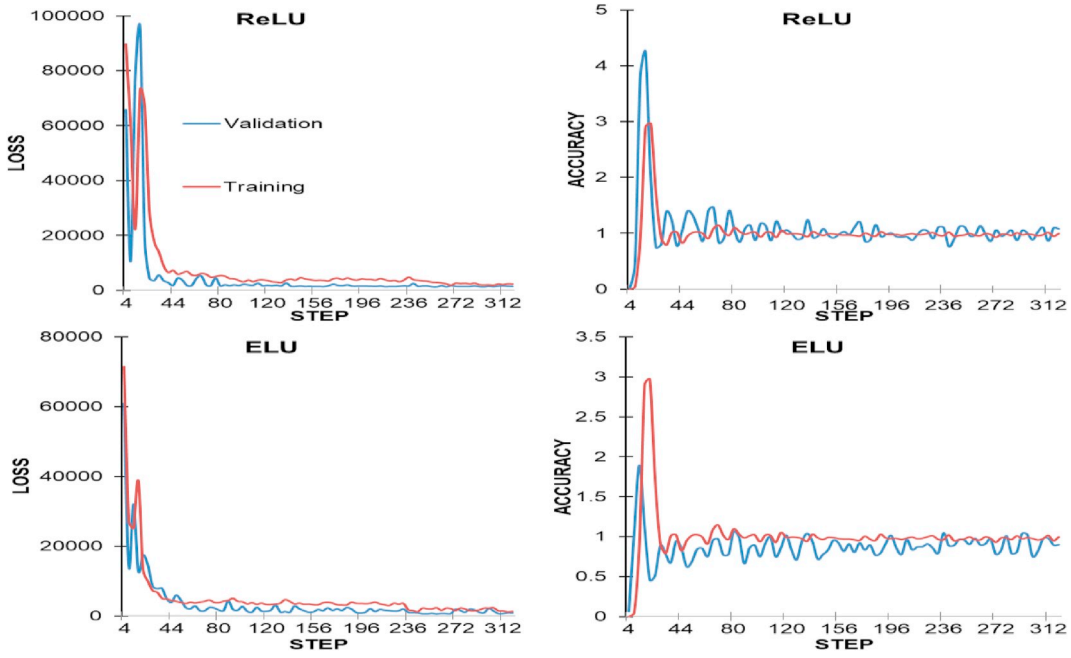

Fig. 5. Loss and accuracy curves of both training and validation processes for ReLU and ELU.

kg/m^3) was statistically higher than that of the healthy subjects (218.75 ± 23.05 kg/m^3). The distributions of surface wave speed at three frequencies and lung mass density of datasets were plotted in Fig. 3. It showed normal distributions of surface wave speed at three frequencies and FEV/FVC%. The distributions of FEV% Pre and density were severely skewed.

The convergence of the two activation functions was illustrated in terms of the training and validation loss over the steps in Figs. 4 and 5. For the ReLU and ELU, training and validation loss significantly decreased as the number of training epochs increased. After 80 epochs (iterations through the entire dataset), the training was stopped due to the absence of further improvement in both accuracy and loss.

MSE and accuracy of the validation dataset of two different activation functions are shown in Table 2. Comparisons of correlation coefficients (R^2) with different activation functions in the DNN and ML for the testing dataset are shown in Table 3. It showed that ELU in the DNN obtained a comparatively better performance.

Table 2
MSE and accuracy of the DNN for different activation functions.

	MSE	Accuracy
ReLU	1532	0.84
ELU	905	0.89

Table 3
The comparison of correlation coefficients (R^2) in both the training and testing datasets using the DNN with ReLU or ELU as well as ML algorithms.

	ReLU	ELU	SVR	Random forest	AdaBoost
Training	0.98	0.96	0.02	0.88	0.87
Testing	0.82	0.89	0.03	0.8	0.76

4. Discussions

The aim of this study was to develop a DNN model to predict lung mass density for ILD patients based on measurements obtained from LUSWE and PFT. The densities of lung tissue covering both ILD patients and healthy subjects were calculated based on the HU obtained from HRCT. It showed that the magnitude of lung mass density of ILD patients was higher than that of healthy subjects. The DNN model was trained with surface wave speeds at three vibration frequencies, FEV1% pre and FEV1%/FVC% from PFT, and predefined lung mass densities from HRCT. The obtained results showed that the DNN with activation function ELU can be used to predict lung mass density with high accuracy.

Predefined lung mass densities of both the ILD patients and healthy subjects based on the HU are in agreement with available information in literature. It has been shown that lung mass density ranges between 240 kg/m^3 and 620 kg/m^3 given lung parenchyma is a porous material filled with air and with a void ratio of roughly 0.7 (Marsh et al., 2007; Hartley et al., 1994; Guenard et al., 1992; Garnett et al., 1977). Results from this study showed that the magnitude of lung mass density of ILD patients was higher than that of healthy subjects. Our previous study showed that the magnitudes of wave speed of the lung surface for ILD patients were also higher than that of healthy subjects (Zhou et al., 1817; Clay et al., 2019). With lung mass density predicted using the DNN model, we can calculate the viscoelasticity of the lung surface using Voigt's model based on surface wave speeds at different vibration frequencies obtained from LUSWE (Zhou and Zhang, 2018b). These measures can be further used to assess disease development and prognosis for ILD patients and develop a lung fibrosis staging system. Moreover, wave speed of anterior, lateral, and posterior spaces of both lungs were measured in LUSWE. With calculated viscoelasticity, we can evaluate the heterogeneity of lung fibrosis for ILD patients. The measurements obtained from LUSWE and PFT were based on human assessment and error prone. However, if the model is well-built and properly trained, this issue could be overcome.

The output of the ReLU is zero across half of its domain making it very quick to train compared with other activation functions. However, the ReLU is subject to the problem of vanishing gradient given its mean output is not zero, introducing a bias for the next layer and slowing down the learning process when used in the DNN. The ELU function is bounded by a fixed value ($-\alpha$) helping to push the mean activation of neurons closer to zero and reducing the influence of noise (Clevert et al., 2015). Given the sample size of the validation set was smaller than that of the training dataset, loss and accuracy of the validation set was comparatively better than those of the training set.

This technique may be used to assess multiple lung disorders such as pulmonary edema when the alveoli are partly filled with blood or fluid. For congestive heart failure and inflammatory conditions, pulmonary edema is a basic characteristic (Soni et al., 2015). Extravascular lung water suggests worse development in critically ill patients and higher risk of heart failure readmission or death (Gargani, 2015). In these 'wet' lungs, ultrasound may penetrate deeper in the diseased tissue than healthy lung tissue, allowing imaging of deeper tissue. The development of a robust, quantitative method for lung mass density analysis has the potential to expand LUSWE in an almost exponential manner across a multitude of clinical applications. For example, quantitative LUSWE could be incorporated into the care of heart failure patients both in hospital practice and in outpatient clinics. In hospital practice, practitioners could perform daily LUSWE on patients undergoing diuresis for congestive heart failure and individually tailor medical therapy based on quantitative changes in LUSWE findings. Since each patient serves as their own reference standard, improvement in lung density through diuresis could be clearly documented and monitored. Outpatient providers could use quantitative LUSWE to monitor for increases in extravascular lung water and implement more timely changes in therapy.

Several limitations in this study should be taken into consideration when interpreting the results. Firstly, this was a retrospective study on a dataset that was available at the time of the study. Further prospective investigation on the use of the DNN in research for lung mass density prediction should be valuable. Secondly, the sample size of the dataset for training is limited, resulting in a small batch size. In the future, we plan to recruit more patients to further validate this technique. Given the limited dataset and high nonlinearity of the DNN model, error in predictions is unavoidable. The error could be further reduced by developing advanced models such as gradient boosting decision tree algorithms (XGBoost) and increasing the pool size of the training dataset. Hyper parameter tuning is a big hurdle in deep learning and making the model explainable is of great importance. In the future, we will use a SHAP (Shapley Additive exPlanations) approach to explain the output of the machine learning model (García and Aznarte, 2019).

5. Conclusion

In this study, we developed a DNN model for mass density prediction of superficial lung tissue based on measurements obtained from LUSWE and PFT. The training of the DNN model was conducted by minimizing the MSE of the training dataset with different activation functions. The proposed technique was evaluated on a dataset of ILD patients and healthy controls. Its performance was compared with those of ML algorithms, and we demonstrated that the DNN was able to predict lung mass density with high accuracy using activation function ELU.

Declaration of competing interest

There is no conflict of interest.

CRediT authorship contribution statement

Boran Zhou: Data curation, Formal analysis, Writing - original draft, Writing - review & editing. **Brian J. Bartholmai:** Data curation, Writing - review & editing. **Sanjay Kalra:** Data curation, Writing - review & editing. **Xiaoming Zhang:** Conceptualization, Data curation, Formal analysis, Writing - original draft, Writing - review & editing.

Acknowledgements

This study is supported by NIH R01HL125234 from the National Heart, Lung and Blood Institute. We would like to thank Mrs. Jennifer Poston for editing this manuscript.

References

Bankier, A.A., et al., 1999. Pulmonary emphysema: subjective visual grading versus objective quantification with macroscopic morphometry and thin-section CT densitometry. Radiology 211 (3), 851–858.
Clay, R., Bartholmai, B.J., Zhou, B., Karwoski, R., Peikert, T., Osborn, T., Rajagopalan, S., Kalra, S., Zhang, X., 2019. Assessment of interstitial lung disease using lung ultrasound surface wave elastography: a novel technique with clinicoradiologic correlates. J. Thorac. Imag. 34 (5), 313–319. https://doi.org/10.1097/RTI.0000000000000334. PMID: 29877916, PMCID: 6281810.
Clevert, D.-A., Unterthiner, T., Hochreiter, S., 2015. Fast and Accurate Deep Network Learning by Exponential Linear Units (Elus) arXiv preprint arXiv:1511.07289.
Coultas, D.B., et al., 1994. The epidemiology of interstitial lung diseases. Am. J. Respir. Crit. Care Med. 150 (4), 967–972.
Drucker, H., et al., 1997. Support vector regression machines. In: Advances in Neural Information Processing Systems.

García, M.V., Aznarte, J.L., 2019. Shapley additive explanations for NO2 forecasting. Ecol. Inf. 101039.
Gargani, L., 2015. Prognosis in heart failure: look at the lungs. Eur. J. Heart Fail. 17 (11), 1086–1088.
Garnett, E., et al., 1977. Lung density: clinical method for quantitation of pulmonary congestion and edema. Can. Med. Assoc. J. 116 (2), 153.
Glorot, X., Bengio, Y., 2010. Understanding the difficulty of training deep feedforward neural networks. In: Proceedings of the Thirteenth International Conference on Artificial Intelligence and Statistics.
Gould, G., et al., 1988. CT measurements of lung density in life can quantitate distal airspace enlargement—an essential defining feature of human emphysema. Am. Rev. Respir. Dis. 137 (2), 380–392.
Guenard, H., et al., 1992. Lung density and lung mass in emphysema. Chest 102 (1), 198–203.
Hakimisefat, B., Mayo, P.H., 2010. Lung ultrasonography. Open Crit. Care Med. J. 3, 21–25.
Hartley, P.G., et al., 1994. High-resolution CT-derived measures of lung density are valid indexes of interstitial lung disease. J. Appl. Physiol. 76 (1), 271–277.
Kazerooni, E.A., Gross, B.H., 2004. Cardiopulmonary Imaging, vol. 4. Lippincott Williams & Wilkins.
Kingma, D., Ba, J., 2014. Adam: A Method for Stochastic Optimization arXiv preprint arXiv:1412.6980.
Kohavi, R., 1995. A study of cross-validation and bootstrap for accuracy estimation and model selection. In: Ijcai (Stanford, CA).
Kornum, J.B., et al., 2008. The incidence of interstitial lung disease 1995-2005: a Danish nationwide population-based study. BMC Pulm. Med. 8, 24.
Kuntz, E., Kuntz, H.-D., 2006. Hepatology, Principles and Practice: History, Morphology, Biochemistry, Diagnostics, Clinic, Therapy. Springer Science & Business Media.
Lepor, H., 2000. Prostatic Diseases, vol. 2000. WB Saunders Company.
Liaw, A., Wiener, M., 2002. Classification and regression by randomForest. R. News 2 (3), 18–22.
Lung Disease Data: 2008, 2008. American Lung Association, New York.
Marsh, S., et al., 2007. Utility of lung density measurements in the diagnosis of emphysema. Respir. Med. 101 (7), 1512–1520.
Mathieson, J.R., et al., 1989. Chronic diffuse infiltrative lung disease: comparison of diagnostic accuracy of CT and chest radiography. Radiology 171 (1), 111–116.
Mayo, J.R., 2009. CT evaluation of diffuse infiltrative lung disease: dose considerations and optimal technique. J. Thorac. Imag. 24 (4), 252–259.
Prim, D.A., et al., 2016. A mechanical argument for the differential performance of coronary artery grafts. J. Mech. Behav. Biomed. Mater. 54, 93–105.
Royston, T.J., et al., 2011. Estimating material viscoelastic properties based on surface wave measurements: a comparison of techniques and modeling assumptions. J. Acoust. Soc. Am. 130 (6), 4126–4138.
Shazly, T., et al., 2015. On the uniaxial ring test of tissue engineered constructs. Exp. Mech. 55 (1), 41–51.
Shin, H.-C., et al., 2016. Deep convolutional neural networks for computer-aided detection: CNN architectures, dataset characteristics and transfer learning. IEEE Trans. Med. Imag. 35 (5), 1285–1298.
Solomatine, D.P., Shrestha, D.L., AdaBoost, R.T., 2004. A boosting algorithm for regression problems. In: 2004 IEEE International Joint Conference on Neural Networks. IEEE Cat. No. 04CH37541 (IEEE).
Soni, N.J., et al., 2015. Ultrasound in the diagnosis & management of pleural effusions. J. Hosp. Med. 10 (12), 811–816.
Sousa, J.C., Jorge, H.M., Neves, L.P., 2014. Short-term load forecasting based on support vector regression and load profiling. Int. J. Energy Res. 38 (3), 350–362.
Tanaka, A., Nakano, T., Ikehara, K., 2011. X-ray computerized tomography analysis and density estimation using a sediment core from the Challenger Mound area in the Porcupine Seabight, off Western Ireland. Earth Planets Space 63 (2), 103–110.
Twal, W.O., et al., 2014. Cellularized microcarriers as adhesive building blocks for fabrication of tubular tissue constructs. Ann. Biomed. Eng. 42 (7), 1470–1481.
Verschakelen, J.A., 2010. The role of high-resolution computed tomography in the work-up of interstitial lung disease. Curr. Opin. Pulm. Med. 16 (5), 503–510.
Volpicelli, G., 2013. Lung sonography. J. Ultrasound Med. 32 (1), 165–171.
Xu, J., Kochanek, K.D., Murphy, S.L., Tejada-Vera, B., 2010. Deaths: final data for 2007. Natl. Vital Stat. Rep. 58 (19), 1–136.
Zeiler, M.D., et al., 2013. On rectified linear units for speech processing. In: Acoustics, Speech and Signal Processing (ICASSP), 2013 IEEE International Conference on. IEEE.
Zhang, X., et al., 2017a. Lung ultrasound surface wave elastography: a pilot clinical study. IEEE Trans. Ultrason. Ferroelectrics Freq. Contr. 64 (9), 1298–1304.
Zhang, X., et al., 2017b. Assessment of interstitial lung disease using lung ultrasound surface wave elastography. In: Ultrasonics Symposium (IUS). IEEE International, 2017.
Zhang, X., et al., 2017c. An ultrasound surface wave elastography technique for noninvasive measurement of surface lung tissue. J. Acoust. Soc. Am. 141 (5), 3721-3721.
Zhang, X., et al., 2018a. An ultrasound surface wave technique for assessing skin and lung diseases. Ultrasound Med. Biol. 44 (2), 321–331.
Zhang, X., et al., 2018b. Lung ultrasound surface wave elastography for assessing interstitial lung disease. J. Acoust. Soc. Am. 143 (3), 1776-1776.
Zhou, B., Zhang, X., 2018a. The effect of pleural fluid layers on lung surface wave speed measurement: experimental and numerical studies on a sponge lung phantom. J. Mech. Behav. Biomed. Mater.
Zhou, B., Zhang, X., 2018b. Comparison of five viscoelastic models for estimating viscoelastic parameters using ultrasound shear wave elastography. J. Mech. Behav. Biomed. Mater. 85, 109–116.
Zhou, B., Zhang, X., 2018c. Lung mass density analysis using deep neural network and lung ultrasound surface wave elastography. Ultrasonics 89, 173–177. https://doi.org/10.1016/j.ultras.2018.05.011. Epub 2018 May 23 PMID: 29852466 PMCID: 6014933.
Zhou, B., et al., Lung US surface wave elastography in interstitial lung disease staging. Radiology. 0(0): p. 181729.